Electronic Supplementary Information
Computational exploration of a Zr-carboxylate based Metal-Organic Framework as a membrane material for CO_2 capture

Dong Wu,[a,b] *Guillaume Maurin,*[*b] *Qingyuan Yang,*[a] *Christian Serre,*[c] *Hervé Jobic,*[d] *and Chongli Zhong*[*a]

[a] State Key Laboratory of Organic-Inorganic Composites, Beijing University of Chemical Technology, Beijing, 100029, China.

[b] Institut Charles Gerhardt Montpellier, Université Montpellier 2, 34095, Montpellier cedex 05, France.

[c] Institut Lavoisier, UMR CNRS 8180-Université de Versailles St Quentin en Yvelines, 45 avenue des Etats-Unis, 78035 Versailles, France.

[d] Institut de Recherches sur la Catalyse et l'Environnement de Lyon, Université de Lyon 1, CNRS, 2. Av. A. Einstein, 69626 Villeurbanne, France.

* Corresponding authors. E-mail: guillaume.maurin@univ-montp2.fr; zhongcl@mail.buct.edu.cn

1. Force field and charges

Table S1. LJ potential parameters and partial charges considered for each adsorbate.

Atomic type	σ **(Å)**	ε **(kJ mol^{-1})**	$q(e)$
CO_2_C	2.757	0.234	0.6512
CO_2_O	3.033	0.669	-0.3256
CH_4	3.730	1.230	0.0000
N_2_N	3.310	0.299	-0.482
N_2_COM	0	0	0.964

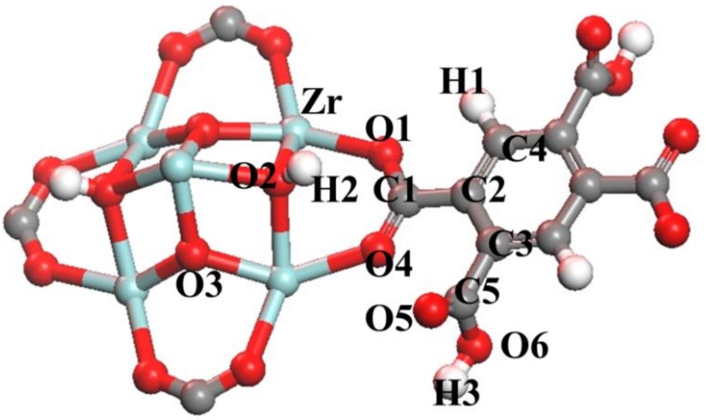

Fig. S1 Atom types for the framework of UiO-66(Zr)-$(COOH)_2$.

Table S2 Lennard-Jones (LJ) potential parameters and charges for all atoms of the UiO-66(Zr)-$(COOH)_2$ framework.

	DREIDING[1]		**UFF**[2]		***Charge(e)***
	σ (Å)	ε (kJ/mol)	σ (Å)	ε (kJ/mol)	
Zr	2.783[a]	0.2887[a]	2.783	0.2887	2.162
C1	3.473	0.3979	3.431	0.4393	0.610
C2	3.473	0.3979	3.431	0.4393	-0.065
C3	3.473	0.3979	3.431	0.4393	-0.034
C4	3.473	0.3979	3.431	0.4393	-0.118
C5	3.473	0.3979	3.431	0.4393	0.703
O1	3.033	0.4004	3.118	0.2510	-0.521
O2	3.033	0.4004	3.118	0.2510	-1.057
O3	3.033	0.4004	3.118	0.2510	-0.949
O4	3.033	0.4004	3.118	0.2510	-0.542
O5	3.033	0.4004	3.118	0.2510	-0.554
O6	3.033	0.4004	3.118	0.2510	-0.570

H1	2.846	0.0636	2.571	0.1841	0.126
H2	2.846	0.0636	2.571	0.1841	0.431
H3	2.846	0.0636	2.571	0.1841	0.409

[a] taken from UFF as the Zr is not available in the DREIDING forcefield.

2. Grand canonical Monte Carlo simulations

Grand canonical Monte Carlo (GCMC) simulations were performed to calculate the adsorption isotherms for each single component in the non modified and functionalized UiO-66(Zr)s at 303 K using our simulation code CADSS (Complex Adsorption and Diffusion Simulation Suite)[3]. During the simulations, adsorbate molecules involved three types of trials: attempts (i) to displace a molecule (translation or rotation), (ii) to create a new molecule, and (iii) to delete an existing molecule. Details on the method can be found elsewhere.[4]

3. Molecular dynamic simulations

The Nosé-Hoover thermostat was employed while the velocity Verlet algorithm was used to integrate the Newton equations. In the same way than the GCMC simulations, the Ewald summation method was considered to evaluate the long-range coulombic interactions and all the LJ interactions were calculated with a cutoff radius of 14.0 Å. The time step used in the MD simulations was taken as 1.0 fs, and periodic boundary conditions were applied in all three dimensions. All the MD simulations were performed using a flexible framework (see section below) as follows: the guest molecules were randomly inserted into the simulation box, and then relaxed using 2×10^5 NVT Monte Carlo cycles. Velocities from the Maxwell-Boltzmann distribution at the required temperature were assigned to all the adsorbate molecules and the framework atoms. Further, the production run of 2×10^7 MD steps (i.e., 20 ns) were performed for each MD calculation after an equilibration of the system with 2×10^6 MD steps. The positions of the adsorbates molecules and the framework atoms were stored every 5000 MD steps for subsequent analysis.

Based on these simulations, both the self-diffusivity (D_s) and corrected diffusivity (D_0) were extracted. The self-diffusivity related to the displacement of a tagged molecule is obtained from the plot of the mean square displacement (MSD) as a function of the time using an Einstein relation[4].

$$D_s(c) = \frac{1}{2dN} \lim_{t\to\infty} \frac{\mathrm{d}}{\mathrm{d}t} \left\langle \sum_{i=1}^{N} \left| \mathbf{r}_i(t) - \mathbf{r}_i(0) \right|^2 \right\rangle \qquad (3\text{-}1)$$

where $\langle \cdots \rangle$ denotes an ensemble average, $\mathbf{r}_i(t)$ is the position vector of the diffusing molecule i at time t, N is the number of adsorbate molecules in the simulation system, and d corresponds to the dimension of the system examined (d=3 for current material).

The corrected diffusivity which measures the MSD of the center of mass of all the adsorbates molecules is also calculated using an Einstein expression defined as above[4].

$$D_0(c) = \frac{1}{2dN} \lim_{t\to\infty} \frac{\mathrm{d}}{\mathrm{d}t} \left\langle \left| \sum_{i=1}^{N} \left[\vec{\mathbf{r}}_i(t) - \vec{\mathbf{r}}_i(0) \right] \right|^2 \right\rangle \qquad (3\text{-}2)$$

The self and correct diffusivities were averaged from five MD independent trajectories for the statistics of the calculation and the method with multiple time origins was also adopted as described previously.[9] Finally, the transport diffusivity (D_t), which is also known as the Fick diffusivity, was calculated from the following expression:

$$D_t(c) = D_0(c) \left(\frac{\partial \ln f}{\partial \ln c} \right)_T \qquad (3\text{-}3)$$

where the term involving the logarithmic derivative of the fugacity (f) vs the loading (c) referred to as the thermodynamic correction factor (Γ), was determined from the adsorption isotherm.

4. Flexible forcefield for the framework of UiO-66(Zr)-(COOH)$_2$

To describe the flexibility of the functionalized framework UiO-66(Zr)-(COOH)$_2$, in line with our previous study, we first selected the consistent valence forcefield (CVFF)[5] where the bond stretches (Eq. 4-1) and bond bending (Eq. 4-2) are expressed by a simple harmonic potential function, while the bond torsion (Eq. 4-3) and improper torsion angles (Eq. 4-4) were described by the periodic cosine potential function.

$$U_{ij}^{bond} = \frac{1}{2} k_{ij} (r_{ij} - r_0)^2 \qquad \text{(4-1)}$$

$$U_{ijk}^{bending} = \frac{1}{2} k_{ijk} (\theta_{ijk} - \theta_0)^2 \qquad \text{(4-2)}$$

$$U_{ijk}^{Torsion} = k_{ijkl} [1 + \cos(n\phi_{ijk} - \phi_0] \qquad \text{(4-3)}$$

$$U_{ijk}^{Improper\ Torsion} = k_{ijkl} [1 + \cos(n\phi_{ijk} - \phi_0] \qquad \text{(4-4)}$$

where k_{ij}, k_{ijk} and k_{ijkl} are the force constants for the various interactions, r_0 is the equilibrium bond length separating two atoms i and j, θ_0 is the equilibrium angle involving three atoms i, j and k, n is the periodicity, ϕ is the dihedral angle and ϕ_0 is the factor phase.

Table S3 Forcefield parameters for the flexible UiO-66(Zr)-(COOH)$_2$ refined in this work. The definitions of the atom types are shown in Fig. S1.

Interaction types (i-j)	**Bond stretches**	
	k_{ij} (kJ mol^{-1} Å^{-2}))	**r_0 (Å)**
Zr-O1	2872.902	2.296
Zr-O4	2872.902	2.277
Zr-O2	1077.338	2.325
Zr-O3	1077.338	2.126
C1-O1	4518.720	1.268
C1-O4	4518.720	1.270
C1-C2	2939.283	1.501
C2-C3	4016.640	1.408
C2-C4	4016.640	1.400
C3-C4	4016.640	1.395
C3-C5	2939.283	1.513
C4-H1	3041.068	1.081
C5-O6	3347.200	1.348
C5-O5	4518.720	1.212
O6-H3	4524.022	0.974
O2-H2	4524.022	1.002
Interaction types (i-j-k)	**Bond bendings**	
	k_{ijk} (kJ mol^{-1} rad^{-2}))	**θ_0 (degree)**
O1-Zr-O2	115.776	71.9
O1-Zr-O2	115.776	140.0
O1-Zr-O1	115.776	124.3
O2-Zr-O2	463.104	135.0
O3-Zr-O4	115.776	83.5
O3-Zr-O4	115.776	141.8

O3-Zr-O3	463.104	89.0
O3-Zr-O2	115.776	85.0
O3-Zr-O1	115.776	83.6
O3-Zr-O1	115.776	141.1
O4-Zr-O4	115.776	123.7
O4-Zr-O2	115.776	72.6
O4-Zr-O2	115.776	139.2
O4-Zr-O1	115.776	75.2
O4-Zr-O1	115.776	79.3
Zr-O1-C1	231.637	134.1
Zr-O4-C1	231.637	134.4
O1-C1-O4	1213.360	125.4
O1-C1-C2	456.013	117.8
O4-C1-C2	456.013	116.9
C1-C2-C3	290.201	120.0
C1-C2-C4	290.201	120.0
C3-C2-C4	753.120	120.0
C2-C3-C4	753.120	120.0
C2-C4-H1	309.616	120.0
C3-C4-H1	309.616	120.0
C2-C3-C5	290.201	120.0
C4-C3-C5	290.201	120.0
C3-C5-O5	456.013	125.4
C3-C5-O6	456.013	111.3
O5-C5-O6	1213.36	123.1
C5-O6-H3	418.400	107.5
Zr-O2-H2	231.637	115.7

Interaction types (i-j-k-l)	**Torsions**		
	k_{ijkl} (kJ mol^{-1})	n	**ϕ_0 (degree)**
Zr-O1-C1-C2	86.837	2	180
Zr-O4-C1-C2	86.837	2	180
O1-C1-C2-C3	5.000	2	180
O1-C1-C2-C4	5.000	2	180
O4-C1-C2-C3	5.000	2	180
O4-C1-C2-C4	5.000	2	180
C1-C2-C3-C4	12.552	2	180
C1-C2-C3-C5	6.000	2	180
C1-C2-C4-C3	12.552	2	180
C1-C2-C4-H1	12.552	2	180
C2-C3-C4-H1	12.552	2	180
C2-C3-C4-C2	12.552	2	180
C2-C4-C3-C5	6.000	2	180

C3-C2-C4-C3	12.552	2	180
C3-C2-C4-H1	12.552	2	180
C3-C4-C2-C3	12.552	2	180
C4-C2-C3-C4	12.552	2	180
C4-C2-C3-C5	6.000	2	180
C5-C3-C4-H1	6.000	2	180
C3-C5-O6-H3	9.414	2	180
O5-C5-O6-H3	9.414	2	180
O2-Zr-O2-H2	86.837	2	180

Interaction types (i-j-k-l)	**Improper torsions**		
	k_{ijkl} (kJ mol^{-1})	n	**ϕ_0 (degree)**
C2-C1-O1-O4	41.840	2	180
C2-C1-O4-O1	41.840	2	180
C1-C2-C3-C4	1.548	2	180
C2-C3-C4-C5	1.548	2	180
C2-C4-C3-H1	1.548	2	180
C3-C5-O5-O6	41.840	2	180

Table S4 Comparison between the simulated structural features of the UiO-66(Zr)-(COOH)$_2$ issued from the MD calculations and those obtained from Density Functional Theory calculations.

Bond length (Å)		
Bond types	**DFT (Å)**	**MD (Å)**
Zr-O1	2.256	2.225
Zr-O2	2.285	2.230
Zr-O3	2.086	2.075
Zr-O4	2.237	2.190
C1-O1	1.268	1.225
C1-O4	1.270	1.225
C1-C2	1.501	1.525
C2-C3	1.408	1.450
C2-C4	1.400	1.425
C3-C4	1.395	1.425
C3-C5	1.513	1.525
C4-H1	1.081	1.075
C5-O5	1.212	1.225
C5-O6	1.348	1.325
O2-H2	0.962	0.975
O6-H3	0.974	0.975

5. Impact of the flexibility of UiO-66(Zr)-(COOH)$_2$ on the diffusivity of CO$_2$

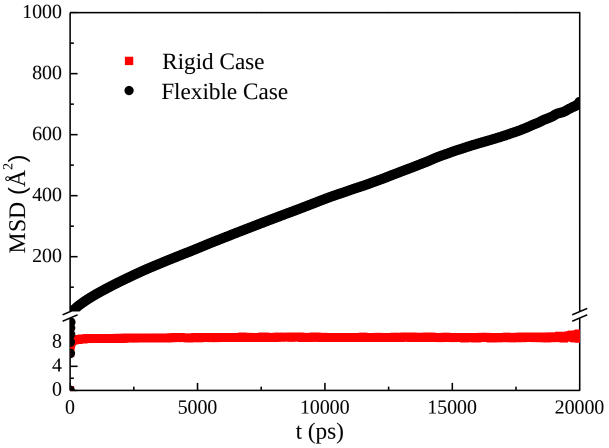

Fig. S2 The MSD of the taggeted CO$_2$ for a loading of 8 molecules/u.c in UiO-66(Zr)-(COOH)$_2$ at 303 K.

From the MD simulations performed for 8 CO$_2$ molecules per unit cell in UiO-66(Zr)-(COOH)$_2$ with a rigid framework, we cannot observe any diffusive molecules for CO$_2$ diffusion within the structure, which can be reflected from the calculated MSD as reported in Fig. S2. Such a constraint can be attributed to the fact that the size of the triangular windows is largely reduced due to the presence of the two carboxylic functional groups on the BDC ligands. However, the quasi-elastic neutron scattering (QENS) measurements demonstrated that the adsorbed molecules at low loadings show evident diffusion processes.[6] Based on the new flexible force field, our MD simulations also showed that the diffusion of the adsorbed molecules is not any more problem and the resulting diffusivity for CO$_2$ is within the same range of values than the experimental data.

6. Adsorption and diffusion of single component CO$_2$, CH$_4$ and N$_2$ in UiO-66(Zr)

6.1 Adsorption

Single component adsorption isotherms were fitted from the simulated data obtained in this work. A dual-site Langmuir model was used to fit the single component adsorption isotherms of CO$_2$, CH$_4$ and N$_2$. The results are shown in Fig. S3 and Table S5.

$$c_i = \frac{a_i f}{b_i + f} + \frac{c_i f}{d_i + f} \tag{6-1}$$

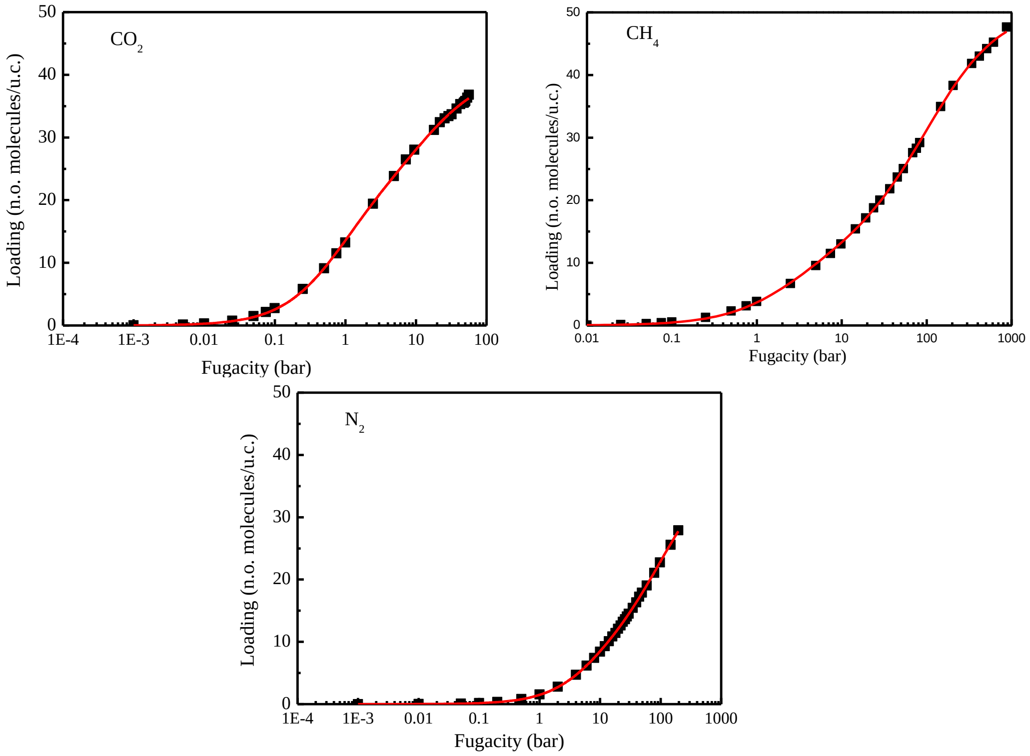

Fig. S3 Single component adsorption isotherms of CO_2 , CH_4 and N_2 in UiO-66(Zr) at 303 K as a function of fugacity. Filled symbols (lines) show results for GCMC simulation (fitted adsorption models).

Table S5. Values and units of single component isotherm parameters.

Parameters	**Values**	**Units**
CO_2		
A	23.22175	molecules/unit cell
B	0.85145	Bar
C	17.12561	molecules/unit cell
D	15.72517	Bar
CH_4		
A	12.73741	molecules/unit cell
B	2.85288	Bar
C	38.30146	molecules/unit cell
D	103.45719	Bar
N_2		
A	11.85841	molecules/unit cell
B	8.34061	Bar
C	26.48697	molecules/unit cell
D	120.70428	Bar

Based on the single-component adsorption isotherms defined above, the adsorption data for the mixture were generated using the Ideal Adsorption Solution Theory (IAST) macroscopic model[7] which were further fitted with a continuous functional form. An extended dual site Langmuir model was then employed to represent the mixtures; the corresponding expressions are given in Equation 6-2 and 6-3 and the parameters are provided in Table S6. The comparisons of the fitting functions used to describe the binary adsorption of mixtures with the IAST-based dataset are also given in Fig. S4.

$$c_i = \frac{a_1 f_i}{a_2 f_i + a_3 f_j + a_4} + \frac{a_5 f_i}{a_6 f_i + a_7 f_j + a_8} \tag{6-2}$$

$$c_j = \frac{b_1 f_j}{b_2 f_i + b_3 f_j + b_4} + \frac{b_5 f_j}{b_6 f_i + b_7 f_j + b_8} \tag{6-3}$$

Table S6. Values and units of extended dual site Langmuir isotherm parameters for CO_2/N_2 and CO_2/CH_4 mixtures.

CO_2	Values	CH_4	Values	Units
a1	8.325877	b1	1.000387	molecules/unit cell
a2	0.478951	b2	0.267148	
a3	0.026550	b3	0.017888	
a4	5.538969	b4	6.097526	bar
a5	9.847699	b5	9.998909	molecules/unit cell
a6	0.448848	b6	4.426079	
a7	0.058531	b7	0.557812	
a8	0.377727	b8	2.176994	bar

CO_2	Values	N_2	Values	Units
a1	1.739574	b1	8.817916	molecules/unit cell
a2	0.074488	b2	9.987688	
a3	0.003440	b3	0.483486	
a4	0.065488	b4	5.616879	bar
a5	9.984710	b5	0.752124	molecules/unit cell
a6	0.593975	b6	0.822095	
a7	0.019852	b7	0.023956	
a8	9.127524	b8	9.997598	bar

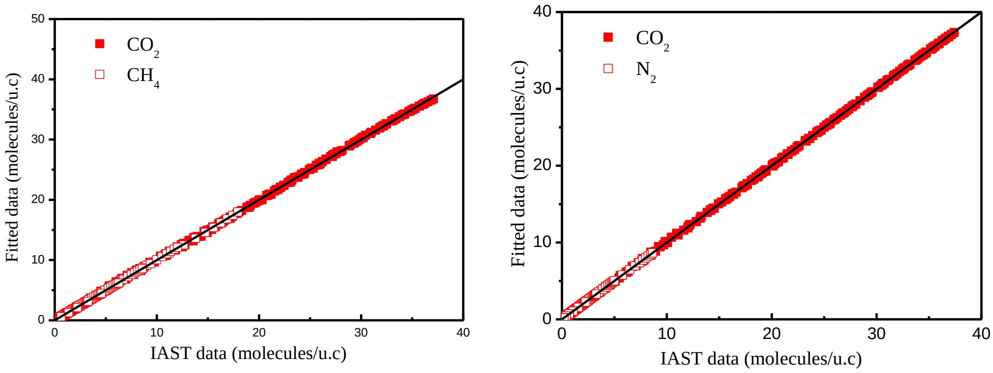

Fig. S4 Comparison of the fitting functions used to describe the binary adsorption of CO_2/CH_4 and CO_2/N_2 in UiO-66(Zr) at 303 K with the IAST-based dataset.

6.2 Diffusion

Continuous functions describing the single component of the self and corrected diffusivities for CO_2, CH_4 and N_2 as a function of their fractional loading are shown in Fig. S5. The functions used are described in Equations 6-4~6-9 and the corresponding parameters are given in Table S7.

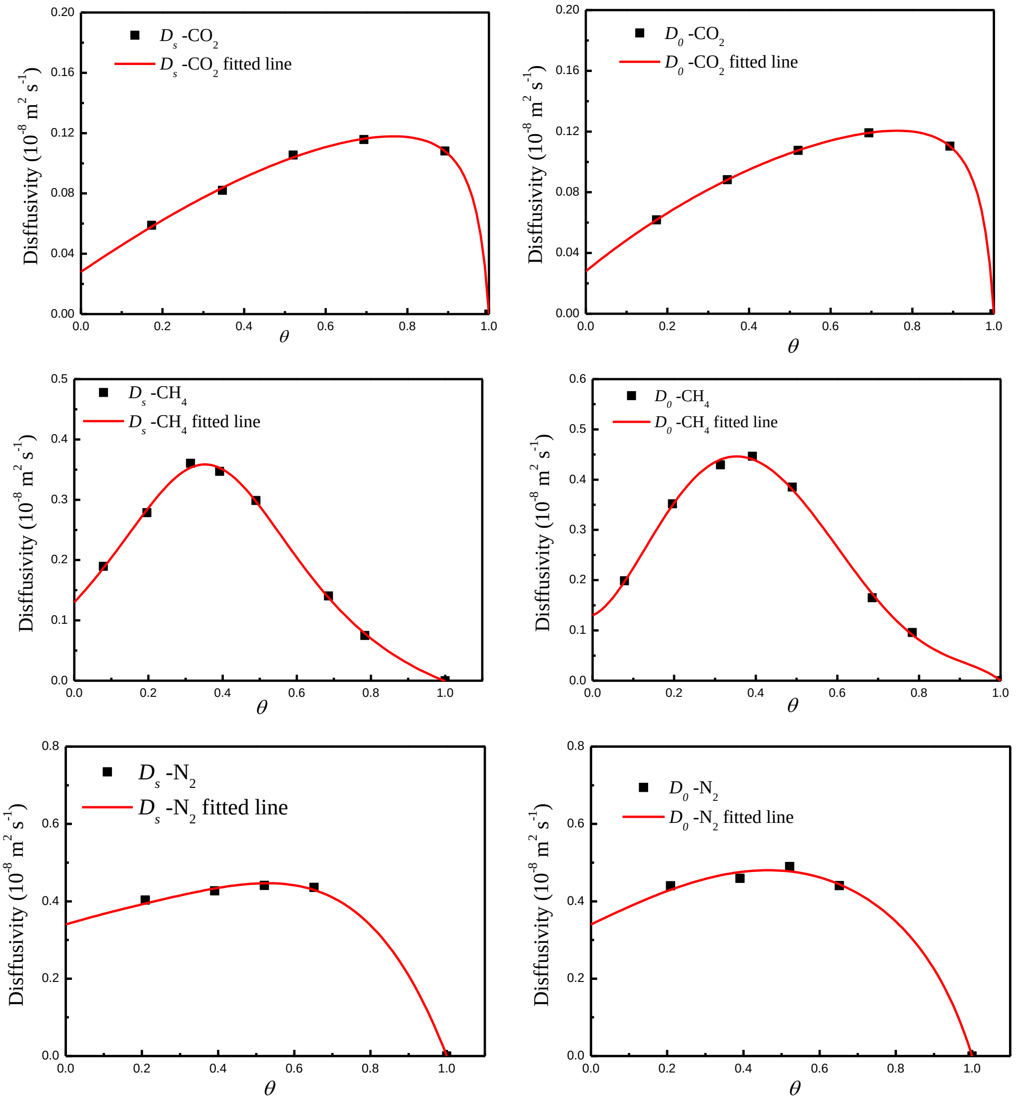

Fig. S5 Self and corrected diffusion coefficients of CO_2, CH_4 and N_2 in UiO-66(Zr) at 303 K. The symbols represent the data from the MD simulations, while the curves show the fitting functions.

$$D_{s,CO_2}(\theta_{CO_2}) = \frac{A_1 + A_3\theta_{CO_2} + A_5\theta_{CO_2}^2}{1 + A_2\theta_{CO_2} + A_4\theta_{CO_2}^2 + A_6\theta_{CO_2}^3} \quad (6\text{-}4)$$

$$D_{0,CO_2}(\theta_{CO_2}) = \frac{B_1 + B_3\theta_{CO_2} + B_5\theta_{CO_2}^2}{1 + B_2\theta_{CO_2} + B_4\theta_{CO_2}^2 + B_6\theta_{CO_2}^3} \tag{6-5}$$

$$D_{s,CH_4}(\theta_{CH_4}) = \frac{R_1 + R_3\theta_{CH_4} + R_5\theta_{CH_4}^2}{1 + R_2\theta_{CH_4} + R_4\theta_{CH_4}^2 + R_6\theta_{CH_4}^3} \tag{6-6}$$

$$D_{0,CH_4}(\theta_{CH_4}) = S_1 + S_2\theta_{CH_4} + S_3\theta_{CH_4}^2 + S_4\theta_{CH_4}^3 + S_5\theta_{CH_4}^4 + S_6\theta_{CH_4}^5 \tag{6-7}$$

$$D_{s,N_2}(\theta_{N_2}) = E_1 + E_2\theta_{N_2} + E_3\theta_{N_2}^2 + E_4\theta_{N_2}^3 + E_5\theta_{N_2}^4 \tag{6-8}$$

$$D_{0,N_2}(\theta_{N_2}) = \frac{F_1 + F_3\theta_{N_2} + F_5\theta_{N_2}^2}{1 + F_2\theta_{N_2} + F_4\theta_{N_2}^2 + F_6\theta_{N_2}^3} \tag{6-9}$$

Table S7. Values and units of the fitted parameters.

CO_2	Values	Units*10^8	CH_4	Values	Units*10^8	N_2	Values	Units*10^8
A1	0.02800	m^2 s^{-1}	R1	0.13000	m^2 s^{-1}	E1	0.34000	m^2 s^{-1}
A2	-0.83062	-	R2	-2.75644	-	E2	0.30115	m^2 s^{-1}
A3	0.15856	m^2 s^{-1}	R3	0.29705	m^2 s^{-1}	E3	-0.34749	m^2 s^{-1}
A4	0.20020	-	R4	3.74712	-	E4	0.97047	m^2 s^{-1}
A5	-0.18656	m^2 s^{-1}	R5	-0.42888	m^2/s	E5	-1.26351	m^2 s^{-1}
A6	-0.31581	-	R6	0.27109	-	-	-	-
B1	0.02800	m^2 s^{-1}	S1	0.13000	m^2/s	F1	0.34000	m^2 s^{-1}
B2	-0.41079	-	S2	0.33247	m^2/s	F2	-1.36756	-
B3	0.20610	m^2 s^{-1}	S3	8.96010	m^2/s	F3	0.01000	m^2 s^{-1}
B4	-0.34195	-	S4	-31.61465	m^2/s	F4	1.18551	-
B5	-0.23410	m^2 s^{-1}	S5	34.97998	m^2/s	F5	-0.35001	m^2 s^{-1}
B6	-0.18292	-	S6	-12.78756	m^2/s	F6	-0.60153	-

7. Adsorption and diffusion of single component CO_2, CH_4 and N_2 in UiO-66(Zr)-(COOH)$_2$

7.1 Adsorption

A dual-site Langmuir model was also used to fit the single component adsorption isotherms of CO_2, CH_4 and N_2 in UiO-66(Zr)-(COOH)$_2$. The results are shown in Fig. S6 and Table S8.

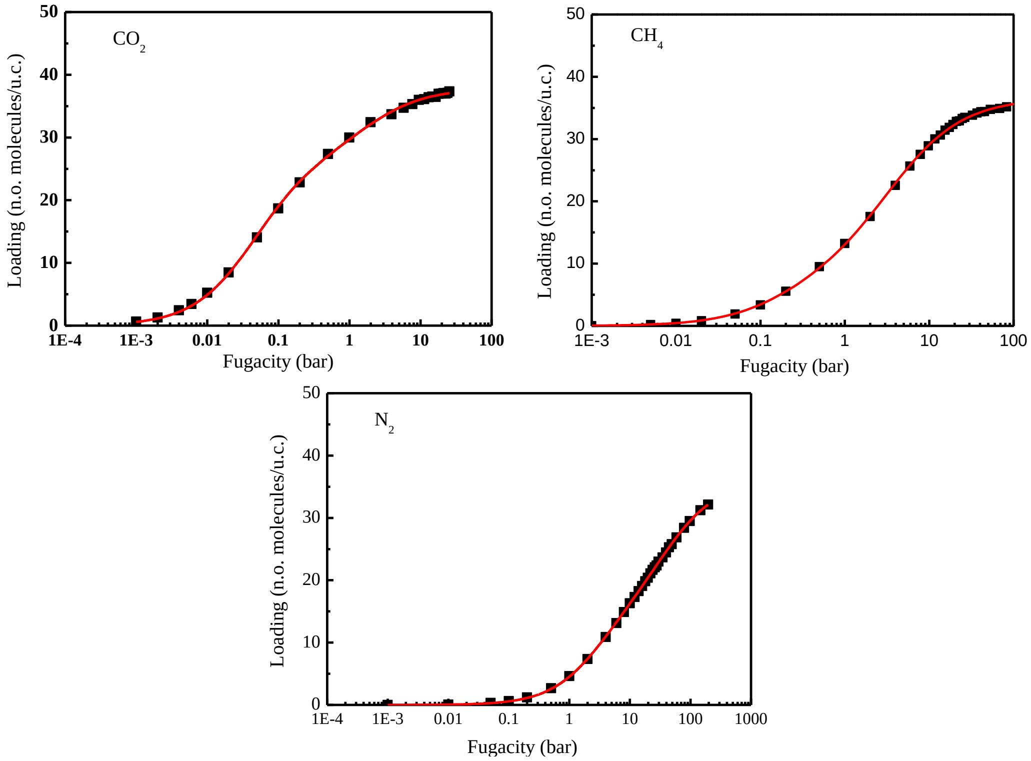

Fig. S6 Single component adsorption isotherms of CO_2 , CH_4 and N_2 in UiO-66(Zr)-$(COOH)_2$ at 303 K as a function of fugacity. Filled symbols (lines) show results for GCMC simulation (fitted adsorption models).

Table S8. Values and units of single component isotherm parameters

Parameters	Values	Units
CO_2		
A	26.84489	molecules/unit cell
B	0.04554	bar
C	10.95622	molecules/unit cell
D	1.73008	bar
CH_4		
A	8.03541	molecules/unit cell
B	0.20434	bar
C	28.5451	molecules/unit cell
D	3.45379	bar
N_2		
A	16.14307	molecules/unit cell
B	2.96602	bar
C	19.69245	molecules/unit cell
D	41.65109	bar

In a similar way than for UiO-66(Zr), an extended dual site Langmuir model was used to model the behavior of the mixtures in UiO-66(Zr)-$(COOH)_2$ and the parameters are shown in Table S9. The comparisons of the fitting functions used to describe the binary adsorption of mixtures with the IAST-based dataset are also given in Fig. S7.

Table S9. Values and units of extended dual site Langmuir isotherm parameters.

CO_2	Values	**CH_4**	Values	Units
a1	9.684151	b1	2.515972	molecules/unit cell
a2	0.906953	b2	2.507446	
a3	0.091872	b3	0.118703	
a4	1.654048	b4	0.057694	bar
a5	4.205899	b5	1.811883	molecules/unit cell
a6	0.154666	b6	1.527678	
a7	0.007515	b7	0.102871	
a8	0.007393	b8	1.268614	bar

CO_2	**Values**	**N_2**	**Values**	**Units**
a1	1.840084	b1	1.595544	molecules/unit cell
a2	0.068495	b2	8.857934	
a3	0.000515	b3	0.078439	
a4	0.003137	b4	0.252175	bar
a5	9.999379	b5	1.094243	molecules/unit cell
a6	0.913892	b6	9.999626	
a7	0.009079	b7	0.000000	
a8	1.583044	b8	9.758847	bar

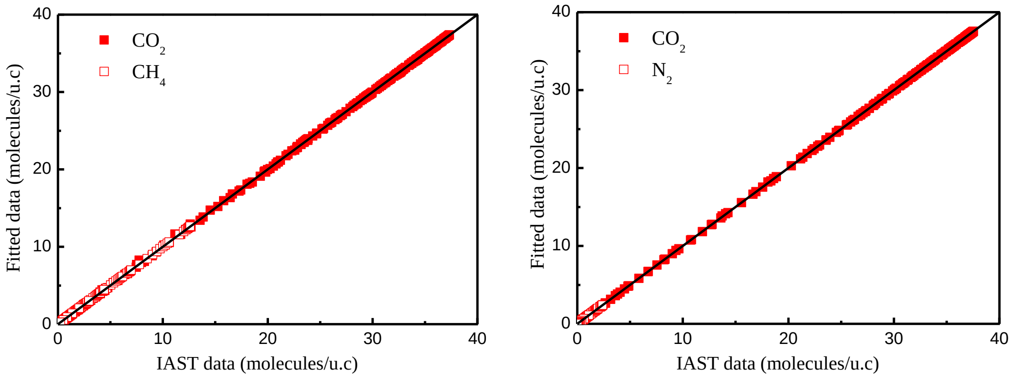

Fig. S7 Comparison of the fitting functions used to describe binary adsorption of CO_2/CH_4 and CO_2/N_2 in UiO-66(Zr)-$(COOH)_2$ at 303 K with the IAST-based dataset used to determine these functions.

7.2 Diffusion

The continuous functions to describe the single component self and corrected diffusivities of CO_2 , CH_4 and N_2 as a function of their fractional loading are shown in Fig. S8. The analytical functions are given in Equations 7-1~7-6 and the corresponding parameters are shown in Table S11.

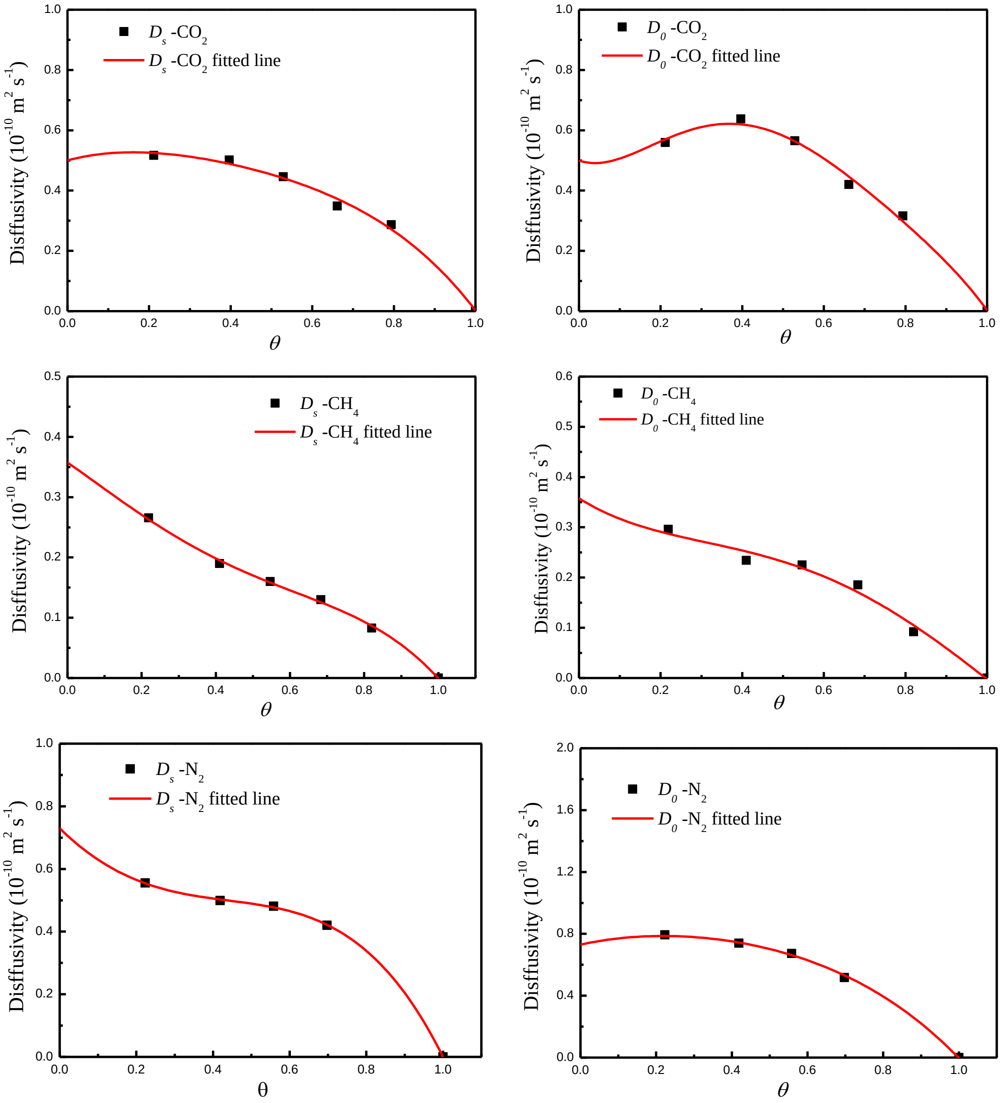

Fig. S8 Self and corrected diffusion coefficients of CO_2, CH_4 and N_2 in UiO-66(Zr)-$(COOH)_2$ at 303 K. Symbols represent the data from the MD simulations, while curves show the fitting functions.

$$D_{s,CO_2}(\theta_{CO_2}) = A_1 + A_2\theta_{CO_2} + A_3\theta_{CO_2}^2 + A_4\theta_{CO_2}^3 + A_5\theta_{CO_2}^4 \tag{7-1}$$

$$D_{0,CO_2}(\theta_{CO_2}) = B_1 + B_2\theta_{CO_2} + B_3\theta_{CO_2}^2 + B_4\theta_{CO_2}^3 + B_5\theta_{CO_2}^4 + B_6\theta_{CO_2}^5 \tag{7-2}$$

$$D_{s,CH_4}(\theta_{CH_4}) = R_1 + R_2\theta_{CH_4} + R_3\theta_{CH_4}^2 + R_4\theta_{CH_4}^3 + R_5\theta_{CH_4}^4 \tag{7-3}$$

$$D_{0,CH_4}(\theta_{CH_4}) = S_1 + S_2\theta_{CH_4} + S_3\theta_{CH_4}^2 + S_4\theta_{CH_4}^3 + S_5\theta_{CH_4}^4 \tag{7-4}$$

$$D_{s,N_2}(\theta_{N_2}) = E_1 + E_2\theta_{N_2} + E_3\theta_{N_2}^2 + E_4\theta_{N_2}^3 + E_5\theta_{N_2}^4 \tag{7-5}$$

$$D_{0,N_2}(\theta_{N_2}) = F_1 + F_2\theta_{N_2} + F_3\theta_{N_2}^2 + F_4\theta_{N_2}^3 + F_5\theta_{N_2}^4 \tag{7-6}$$

Table S11. Values and units of fitted parameters.

CO_2	Values	Units*10^{10}	CH_4	Values	Units*10^{10}	N_2	Values	Units*10^{10}
A1	0.50000	m^2 s^{-1}	R1	0.35765	m^2 s^{-1}	E1	0.73000	m^2 s^{-1}
A2	0.37231	m^2 s^{-1}	R2	-0.43316	m^2 s^{-1}	E2	-1.20881	m^2 s^{-1}
A3	-1.51913	m^2 s^{-1}	R3	-0.15307	m^2 s^{-1}	E3	2.17825	m^2 s^{-1}
A4	1.69992	m^2 s^{-1}	R4	0.84832	m^2 s^{-1}	E4	-1.19491	m^2 s^{-1}
A5	-1.05085	m^2 s^{-1}	R5	-0.62053	m^2 s^{-1}	E5	-0.50462	m^2 s^{-1}
B1	0.5000	m^2 s^{-1}	S1	0.35765	m^2 s^{-1}	F1	0.73000	m^2 s^{-1}
B2	-0.48497	m^2 s^{-1}	S2	-0.50974	m^2 s^{-1}	F2	0.54217	m^2 s^{-1}
B3	7.29392	m^2 s^{-1}	S3	1.18708	m^2 s^{-1}	F3	-1.47241	m^2 s^{-1}
B4	-20.10519	m^2 s^{-1}	S4	-1.64988	m^2 s^{-1}	F4	0.90790	m^2 s^{-1}
B5	19.65337	m^2 s^{-1}	S5	0.6123	m^2 s^{-1}	F5	-0.71168	m^2 s^{-1}
B6	-6.85443	m^2 s^{-1}						

8. Comparison of the diffusivities of CO_2 in UiO-66(Zr) and UiO-66(Zr)-$(COOH)_2$

Fig. S9 compares the simulated self, corrected and transport diffusivities of CO_2 over a wide range of loading in UiO-66(Zr) and its modified form with two carboxylic groups. Obviously, in both MOF structures, the three kinds of diffusivities show similar trends as a function of loading, and the functionalization leads to diffusivities about one order of magnitude lower than those in the non-modified material. The slower diffusion in UiO-66(Zr)-$(COOH)_2$ can be explained from the integral contribution of two factors: (i) polar free carboxylic groups that are prone to strongly interact with CO_2 molecules, which can be supported from the higher low-coverage adsorption enthalpies (–36.4 kJ mol^{-1}) in UiO-66(Zr)-$(COOH)_2$ than that in UiO-66(Zr) (–26.2 kJ mol^{-1}), and (ii) the entropy effect enhanced by the reduced size of windows in the structure of UiO-66(Zr)-$(COOH)_2$. In addition, Fig. S9 shows that the self-diffusivity in UiO-66(Zr)-$(COOH)_2$ exhibits a decreasing trend with increasing loading, which means that the confinement already plays a role at low loading and the packing effect leads to a more evident decrease at higher loadings.

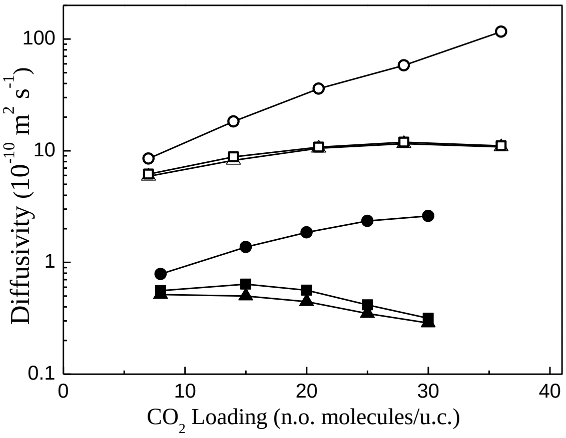

Fig. S9 Comparison of the self-diffusivity *Ds* (triangles), corrected diffusivity D_0 (squares) and transport diffusivity D_t (circles) of CO_2 in the two MOF structures with the evolution of loading. Filled and empty symbols represent UiO-66(Zr)-$(COOH)_2$ and UiO-66(Zr), respectively.

9. Calculation of the performance of pure membranes

The method introduced by Skoulidas, Sholl, and Krishna (SSK) was used to predict the mixture transport diffusivities of binary mixtures in MOFs.[8] This approach combines information from the loading-dependence of the single component self and corrected diffusivities with the binary adsorption isotherms in order to further predict the loading- and composition-dependent matrix of binary diffusion coefficients.This method has been widely used in the prediction of mixture diffusivity for a series of membranes. [9]

To apply the SSK method, it is necessary to first describe the adsorption and diffusion single component behavior of each species. Single component adsorption isotherms were first obtained from GCMC simulations, and continuous functions (dual-site Langmuir model) were fitted to each single component data. Then, IAST was used to predict the adsorption of mixtures. The self and corrected diffusivities of each single component at various loadings were calculated based on MD simulations and fitted as a function of their fractional loading, then SSK theory was used to predict the mixture diffusion in the MOF.The matrix of fick diffusivities $[\mathbf{D}]$ is related to the correlation factors $[\mathbf{B}]$ and to the matrix of thermodynamic correlation factors $[\Gamma]$.

$$[\mathrm{D}]=[\mathrm{B}]^{-1}[\Gamma] \tag{8-1}$$

The steady-state flux of the mixtures was calculated by specifing the pressure and composition on the feed side and the pressure of the permeate side of the membrane.[10] For a binary mixture, it can be written:

$$\begin{bmatrix} N_1 \\ N_2 \end{bmatrix} = -\rho \begin{bmatrix} D_{11} & D_{12} \\ D_{21} & D_{22} \end{bmatrix} \begin{bmatrix} \nabla c_1 \\ \nabla c_2 \end{bmatrix} \tag{8-2}$$

The permeation selectivity is then calculated by the following equation

$$S_{perm,1/2} = \frac{N_1 / N_2}{f_1 / f_2} \tag{8-3}$$

where N_1 and N_2 represent the stead-state fluxes of components *A* and *B* crossing the membrane, respectively; $[\mathbf{D}]$ is the matrix of Fick diffusivities ; ρ is the crystal density of the porous material, ∇c_1 and ∇c_2 are the gradients of the loadings for the components; f_1 and f_2 are the partial gas phase fugacities of the components in the upstream compartment of the membrane.

The permeability P_i of the component *A* and *B* can be extracted by

$$P_i = \frac{N_i}{\Delta p_i} L \tag{8-4}$$

where N_i represents the stead-state fluxes of components *A* and *B* crossing the membrane, respectively; Δp_i is the corresponding pressure drop of components *A* and *B*; *L* is the membrane thickness, which is assumed to be 10 μm in this study.

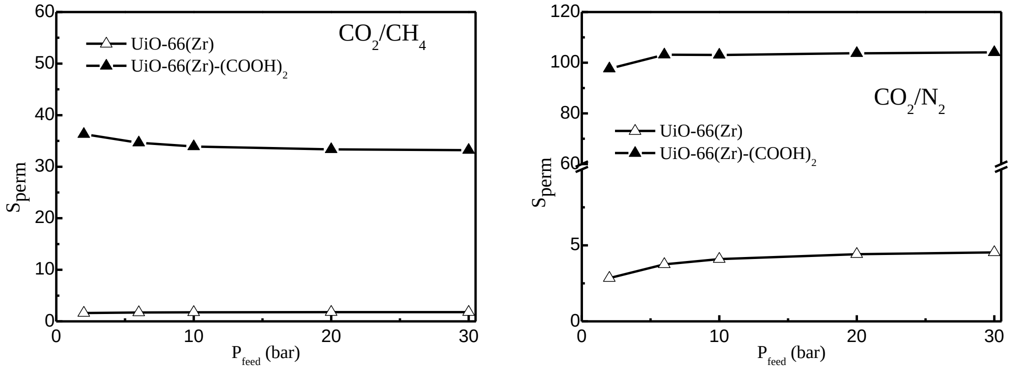

Fig. S10 Mixture permeation selectivities for CO_2/CH_4 and CO_2/N_2 in UiO-66(Zr)-(COOH)$_2$ and UiO-66(Zr) at 303 K as a function of feed pressure(permeate side is vacuum).

10. Mixed matrix membranes (MMMs)

To predict the mixture permeation through MMMs, the dual mode/partial immobilization model[11] was used to predict the permeabilities of CO_2, CH_4 and N_2 in their mixtures through the two polymer membranes poly(1-trimethylsilyl-1-propyne) (PTMSP)[12] and polyimide (TADATO/DSDA(1/1)–DDBT copolyimide)[13] :

$$P_i = k_{Di} D_{Di} \left(1 + \frac{F_i K_i}{1 + \sum_{i=1}^{n} b_i f_i} \right) \tag{9-1}$$

where P_i is the permeability of species i in the mixtures; f_i is the partial pressure of species i in the feed side of the membrane, and the remaining variables are the parameters of the guest species in the two polymers. These parameters can be found in the references 12 and 13.

Once the permeabilities of CO_2/CH_4 and CO_2/N_2 mixtures in polymers and MOFs are known, the Maxwell model was used to predict the mixture permeabilities for MMMs, and then the selectivity is the ratio of gas permeability for each species. The Maxwell model is as follows[14] :

$$\mathrm{P}_r = \frac{P}{P_m} = \left[\frac{2(1-\varphi) + (1+2\varphi)\lambda_{dm}}{(2+\varphi) + (1-\varphi)\lambda_{dm}} \right] \tag{9-2}$$

In this model, P is the permeability of the MOF/polymer MMM, λ_{dm} is the permeability ratio of the dispersed (P_d) and continuous (P_m) phase, P_r is the relative permeability and φ is the volume fraction of dispersed MOF particles.

References:

1. A. K. Rappé, C. J. Casewit, K. S. Colwell, W. A. Goddard III and W. M. Skiff, *J. Am. Chem. Soc.*, 1992, **114**, 10024.
2. S. L. Mayo, B. D. Olafson and W. A. Goddard III, *J. Phys. Chem.*, 1990, **94**, 8897.
3. Q. Yang and C. Zhong, *J. Phys. Chem. B*, 2006, **110**, 17776.

4. D. Frenkel and B. Smit, Understanding Molecular Simulation, Academic Press, 2002, San Diego.

5. P. Dauber-Osguthorpe, V. A. Roberts, D. J. Dauber-Osguthorpe, J. Wolf, M. Genest and A. T. Hagler, *Proteins*, 1988, **4**, 31.

6. Q. Yang, S. Vaesen, F. Ragon, A. D. Wiersum, D. Wu, A. Lago, T. Devic, C. Martineau, F. Taulelle, P. L. Llewellyn, H. Jobic, C. Zhong, C. Serre, G. D. Weireld, and G. Maurin, *Angew. Chem. Int. Ed.*, 2013,**52**, 10316.

7. A. L. Myers and J. M. Prausnitz. *AIChE J.*, 1965, 11, 121

8. A. I. Skoulidas, D. S. Sholl and R. Krishna, *Langmuir*, 2003, **19**, 7977.

9. S. Keskin, J. Liu, J. K. Johnson, and D. S. Sholl, *Langmuir*, 2008, **24**, 8254; S. Keskin, J. Liu, J. K. Johnson, and D. S. Sholl, *Micropor. Mesopor. Mater.*, 2009, **125**, 101.

10. S. Keskin and D.S. Sholl, *Ind. Eng. Chem. Res.*, 2009, ***48***, *914.*

11. D. Q. V**u,** W. J. Koros and S. J. Miller, *J. Membr. Sci.*, 2003, **211**, 335.

12. *T. C. Merkel, V. Bondar,* K. Naga**i a**nd B. D. Freeman, *J. Polym. Sci. Part B: Polym. Phys.*, 2000, **38,** 273.

13. **L**. Yang, J. Fang, N. Meichin, K. Tanaka, H. Kita, K. Okamoto, *Polymer*, 2001, **42**, 2021.

14. J. C. Maxwell, *Treatise on Electricity and Magnetism*, Oxford University Press, London, 1873.